Asian Journal of Chemistry; Vol. 37, No. 4 (2025), 830-836

ASIAN JOURNAL OF CHEMISTRY

https://doi.org/10.14233/ajchem.2025.33405

Synthesis and Characterization of $FeWO_4$/BiOCl Nanocomposites for Photocatalysis and Cytotoxicity in CHO Cell Line

MOHAMMAD FARHAN[1], ANIL KUMAR SINGH[1] and GANDHARVE KUMAR[2,*]

[1]Department of Chemistry, Faculty of Engineering, Teerthanker Mahaveer University, Moradabad-244001, India
[2]Department of Chemistry, School of Basic Sciences, Galgotias University, Greater Noida-203201, India

*Corresponding author: E-mail: gandharve.kumar@galgotiasuniversity.edu.in

Received: 22 January 2025; *Accepted*: 26 February 2025; *Published online*: 29 March 2025; AJC-21943

A novel $FeWO_4$/BiOCl nanocomposite was prepared by hydrothermal route of synthesis and characterized by high-resolution transmission electron microscopy (HRTEM), field-emission scanning electron microscopy (FESEM), powder X-ray diffraction (pXRD) and UV-visible diffuse reflectance spectroscopy (UV-Vis DRS). Photocatalytic activity was evaluated by photocatalytic degradation of rhodamine B (RhB) under the irradiation of visible light. The biological activities such as cytotoxicity were investigated by propidium iodide (PI), a fluorescent dye, uptake and cellular uptake studies. The 15 wt.% $FeWO_4$/BiOCl photocatalysts degraded 98% (RhB, 10 wt.%), whose degradation rate was 3.92 times and 7.34 times higher than that of BiOCl and $FeWO_4$ photocatalysts, respectively. The synthesized $FeWO_4$/BiOCl nanocomposite showed the cytotoxicity to Chinese Hamster Ovary (CHO) cells at concentration increase from 1 µg/mL to 75 µg/mL. In case of cellular uptake studies, $FeWO_4$/BiOCl nanoparticles shows decreases cell viability after 24 h of exposure, as the concentration increase from 1-100 µg/mL.

Keywords: Z-scheme, Hydrothermal method, Solar photocatalyst, Dye degradation.

INTRODUCTION

Due to rapid industrialization, water pollution and energy shortage become the major problem across the world [1,2]. Among various environmental problems, contamination of water bodies by residual textile pollutant is off major concern. Cationic dyes such as rhodamine B have found numerous applications in the field of textile industries and other fabric industries [3-4]. The high retention rate of these dyes in water bodies make them so problematic and hazardous water pollutant. The contamination of both surface and ground water by these cationic dyes has adverse effects on the health of humans and animal [6,7]. Several methods have been employed to eliminate these dyes, with semiconductor-based heterogeneous photocatalysts demonstrating considerable promise in the decontamination of wastewater. However, these photocatalysts face specific challenges, including diminished redox properties, inherent defects, and a high rate of charge carrier recombination [8,9]. Therefore, the design and development of an efficient solar light sensitive semiconductor photocatalyst with enhanced stability and better efficiency for the degeneration of dyes in water under exposure of sunlight is a major approach across the scientific community of world.

Recently, number of bismuth based photocatalyst shows major attention due to their layered structure and efficient visible light responsive nature [10]. Bi-based photocatalyst such as Bi_2WO_6 [11], $BiVO_4$ [12], Bi_2MoO_6 [13] and Bi_2S_3 [14] shows major attention because of their Bi^{3+} ion have full $6s^2$ electronic configuration. BiOCl has been considered as a potential photocatalyst due to its unique structure, non-toxicity, eco-friendly nature with excellent chemical stability [15]. One of the intrinsic drawback of pristine BiOCl is wide band gap, which facilitates the rapid recombination of photoexcited charge carriers, but this issue can be mitigated through the implementation of various design strategies [16]. With a view to overcome these drawbacks, development of Z-scheme based nanocomposites along with semiconductors consisting compatible valence and conduction with respect to BiOCl [17]. The development of a Z-scheme based nanocomposite is valuable from a photocatalytic perspective as it reduces charge carrier recombination

rate and comprising robust redox capabilities. This happens because electrons and holes present in heterostructure are preserved in thermodynamic favourable situation *i.e.*, electron reside in one semiconductor's conduction band and holes in other semiconductor's valence band, which then participate in the redox chemical reactions forming *in situ* reactive oxygen species responsible for the degradation processes [14]. Zhang *et al.* [18] developed a Ag loaded ZnO/BiOCl photocatalyst, which demonstrates enhanced photocatalytic activity towards the antibiotics photodegradation. Grilla *et al.* [17] synthesized a MoS_2/BiOCl heterojunction with type-II scheme, which demonstrates superior photocatalytic potential toward the photocatalytic eradication of antibiotics [17]. Similarly, Meng *et al.* [19] designed a novel $FeWO_4$/BiOCl photocatalyst with Z-scheme heterojunction, which effectively removes the tetracycline.

The photocatalytic activity of BiOCl can be easily enhanced by using $FeWO_4$ as a sensitizer due to compatible band edges of $FeWO_4$ and BiOCl [16,20]. Herein, a novel $FeWO_4$/BiOCl heterostructure *via* a two-step hydrothermal step is developed. By analyzing the morphological, structural and optical properties of as-prepared nanocomposites, were investigated. The plausible development of a Z-scheme type heterostructure among $FeWO_4$ and BiOCl has been outlined. The $FeWO_4$/BiOCl nanocomposites exhibited excellent degradation efficiency towards the removal of rhodamine B dye under exposure of natural sunlight.

EXPERIMENTAL

Chemicals used in this work were ferrous chloride, sodium tungstate, potassium chloride, sodium hydroxide, bismuth nitrate pentahydrate, fetal bovine serum (FBS), antibiotic and antimycotic solution (10,000 µmL penicillin, 10 mg/mL streptomycin and 25 µg/mL amphotericin B) was procured from Life Technologies (India) Pvt. Ltd. New Delhi, India and GIBCO Hams F-12 culture media powder (with L-glutamine, non-essential amino acids and sodium bicarbonate), 0.25% Trypsin-EDTA solution purchased from GIBCO, phosphate buffered saline from GIBCO, propidium iodide purchased from Sigma- Aldrich.

Synthesis of $FeWO_4$ nanoparticles: Firstly, hydrothermal method was used for the synthesis of $FeWO_4$ nanoparticles. Solution A consisted of 5 mmol $FeCl_3{\cdot}6H_2O$ in 25 mL deionized water was added dropwise into solution B comprising of 5 mmol $Na_2WO_4{\cdot}2H_2O$ in 25 mL deionized water and stirred for 30 min. The pH was adjusted to 8 with 1 M NaOH solution carefully. The suspension was put into Teflon-lined stainless autoclave and placed in an oven at 200 ºC for 12 h. Finally, the powdered material was separated out overnight at 50 ºC.

Synthesis of $FeWO_4$/BiOCl photocatalyst: Hydrothermal method was used for the synthesis of $FeWO_4$/BiOCl nanocomposite. Initially, KCl (2 mmol) and $Bi(NO_3)_3{\cdot}5H_2O$ (2 mmol) were mixed in 50 mL ethylene glycol and the reaction mixture was stirred for 30 min. Then, certain amount of $FeWO_4$ (10, 15 and 20 wt.%) was added and the reaction mixture was allowed to stirred for 1 h. Finally, the reaction mixture was put into an autoclave (Teflon-lined) and heated for 12 h at 100 ºC. The prepared sample of $FeWO_4$/BiOCl nanocomposites were filtered followed by washing with water as well as ethanol 5 to 6 times and finally dried overnight. The batches of $FeWO_4$/BiOCl nanocomposites were represented as 10 wt.% $FeWO_4$/BiOCl, 15 wt.% $FeWO_4$/BiOCl and 20 wt.% $FeWO_4$/BiOCl based on amount of $FeWO_4$ precursor added. Similarly, pure BiOCl was synthesized without using $FeWO_4$.

RESULTS AND DISCUSSION

XRD studies: The phase composition of 15 wt.% $FeWO_4$/BiOCl, along with respective individual pristine components, *e.g.* $FeWO_4$ and BiOCl were analyzed by XRD method and the results are presented in Fig. 1. The pristine BiOCl and $FeWO_4$ exhibit XRD patterns that are consistent with tetragonal phase (JCPDS No. 06-0249) and monoclinic phase (JCPDS No. 46-1446), respectively [16,21]. The characteristic diffraction peak of $FeWO_4$ were observed in the best performing photocatalyst *i.e.* 15 wt.% $FeWO_4$/BiOCl nanocomposite.

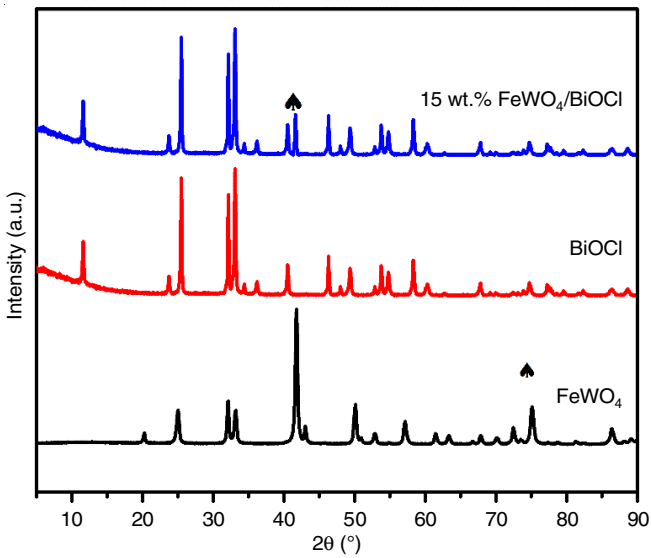

Fig. 1. XRD patterns of BiOCl, $FeWO_4$ and 15 wt.% $FeWO_4$/BiOCl nanocomposite

Morphological studies: The microstructures and sizes of pristine $FeWO_4$ and BiOCl and 15 wt.% $FeWO_4$/BiOCl heterostructure were explored by scanning electron microscopy. The SEM image of $FeWO_4$ discloses the development of a nanoparticles of non-uniform sizes diameters ranging from 80-100 nm (Fig. 2a). While the SEM image of BiOCl displayed a non-uniform nanosheet-like structures of dimensions ranging between 1-2 µm (Fig. 2b). The FESEM image of 15 wt.% $FeWO_4$/BiOCl revealed nanoparticles of $FeWO_4$ adhered to the surface of BiOCl, which appears like a nanosheet morphology (Fig. 2c). The HRTEM image of $FeWO_4$ shows the image of nanoparticles of size 10-20 nm. Further the HRTEM images of 15 wt.% $FeWO_4$/BiOCl hetero-structure shows that the $FeWO_4$ nanoparticles were dispersed on the BiOCl nanosheets (Fig. 2e-g). The size, morphology and hierarchical structure of $FeWO_4$/BiOCl were remains retained as pristine BiOCl.

UV-vis DRS studies: The UV-vis DRS studies were utilized for the determination of band gap of 15 wt.% $FeWO_4$/BiOCl along with $FeWO_4$ and BiOCl. Fig. 3a discloses that pristine BiOCl and the $FeWO_4$/BiOCl strongly absorb in the UV region

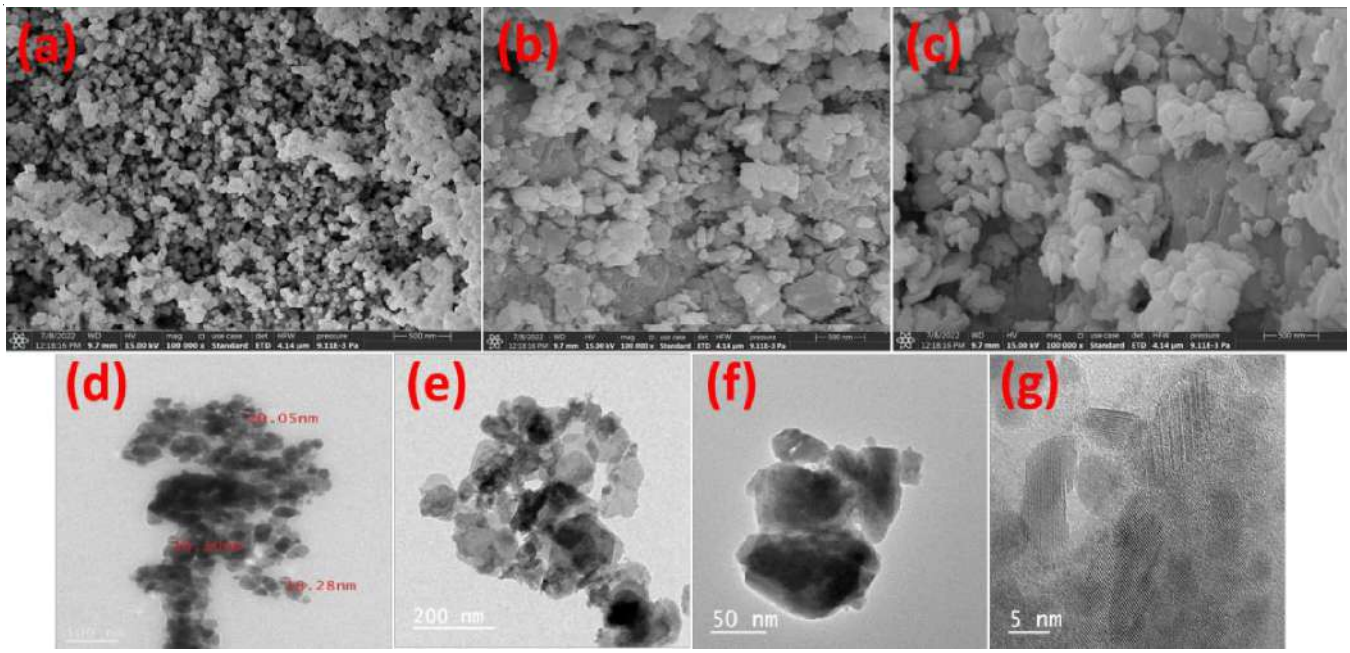

Fig. 2. FESEM image of (a) $FeWO_4$; (b) BiOCl; (c) 15 wt.% $FeWO_4$/BiOCl nanocomposite; HRTEM images of (d) $FeWO_4$, (e-g) 15 wt.% $FeWO_4$/BiOCl

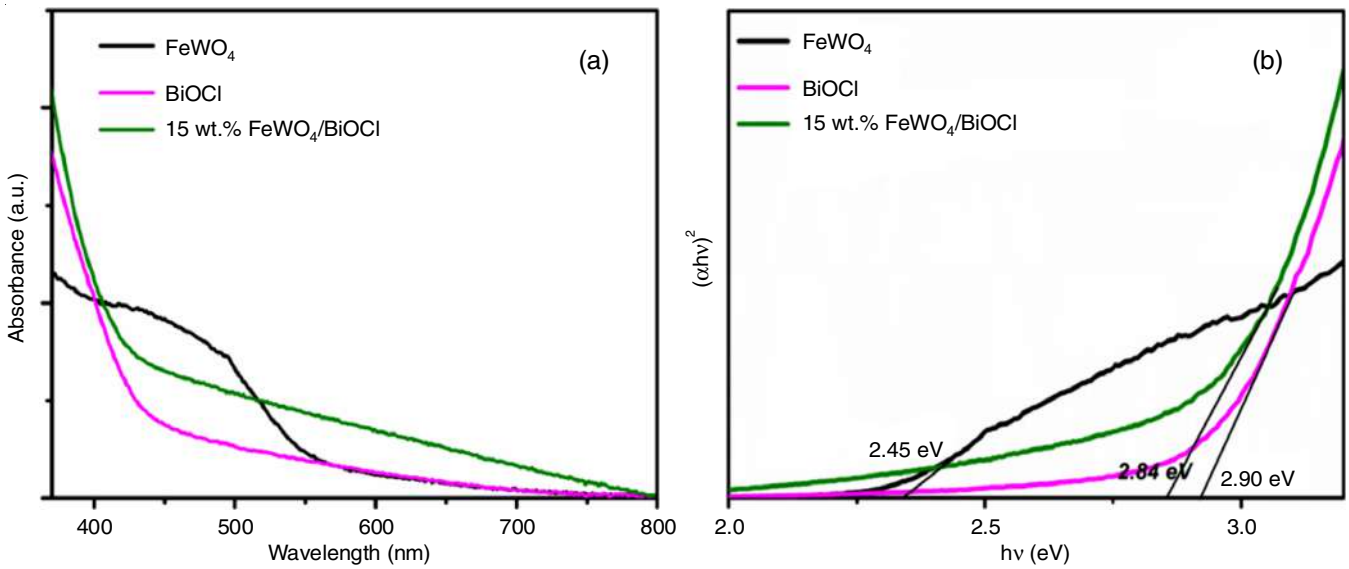

Fig. 3. (a) UV-Vis DRS spectra of $FeWO_4$, BiOCl and 15 wt.% $FeWO_4$/BiOCl nanocomposites, (b) relative band gap energy of $FeWO_4$, BiOCl and 15 wt.% $FeWO_4$/BiOCl

expanding to the visible light region, whereas $FeWO_4$ absorbs solely in the solar region, as represented in Fig. 3a. The band gap energies of $FeWO_4$, BiOCl and 15 wt.% $FeWO_4$/BiOCl are determined from the Tauc plots as 2.45 eV, 2.90 eV and 2.84 eV, respectively (Fig. 3b). The value of conduction and valence band were calculated from the following formula:

$$E_{VB} = \chi - E_e + 1/2\ E_g \quad (1)$$

$$E_{CB} = E_{VB} - E_g \quad (2)$$

The E_{CB} represent energy of conduction band and E_{VB} shows energy of valence band and E_g represents band gap energy, χ values for $FeWO_4$ and BiOCl were 4.45 eV and 6.20 eV , respectively and E_e (energy of free electron) value is 4.5 eV. The conduction band (E_{CB}) and valence band (E_{VB}) values of BiOCl were found to be 0.25 eV and 3.15 eV. Similarly, the values of conduction band (E_{CB}) and valence band (E_{VB}) of $FeWO_4$ were -1.28 eV and 1.17 eV.

Photocatalyst study: The UV-visible absorbance spectra of 10 wt.% of RhB treated with photocatalyst dose of 1 mg/mL, under dark and followed by visible light exposure are shown in Fig. 4a. Fig. 4b shows the plot of C_t/C_0 *versus* time (t). The data corresponding to the photocatalytic degradation under visible light is fitted linearly with first order kinetics as shown in Fig. 4c. The photolysis, *i.e.* RhB without treating with photocatalyst is negligible (Fig. 4b). The optimization of photocatalyst dosage and RhB concentration are mentioned in Fig. 5. The

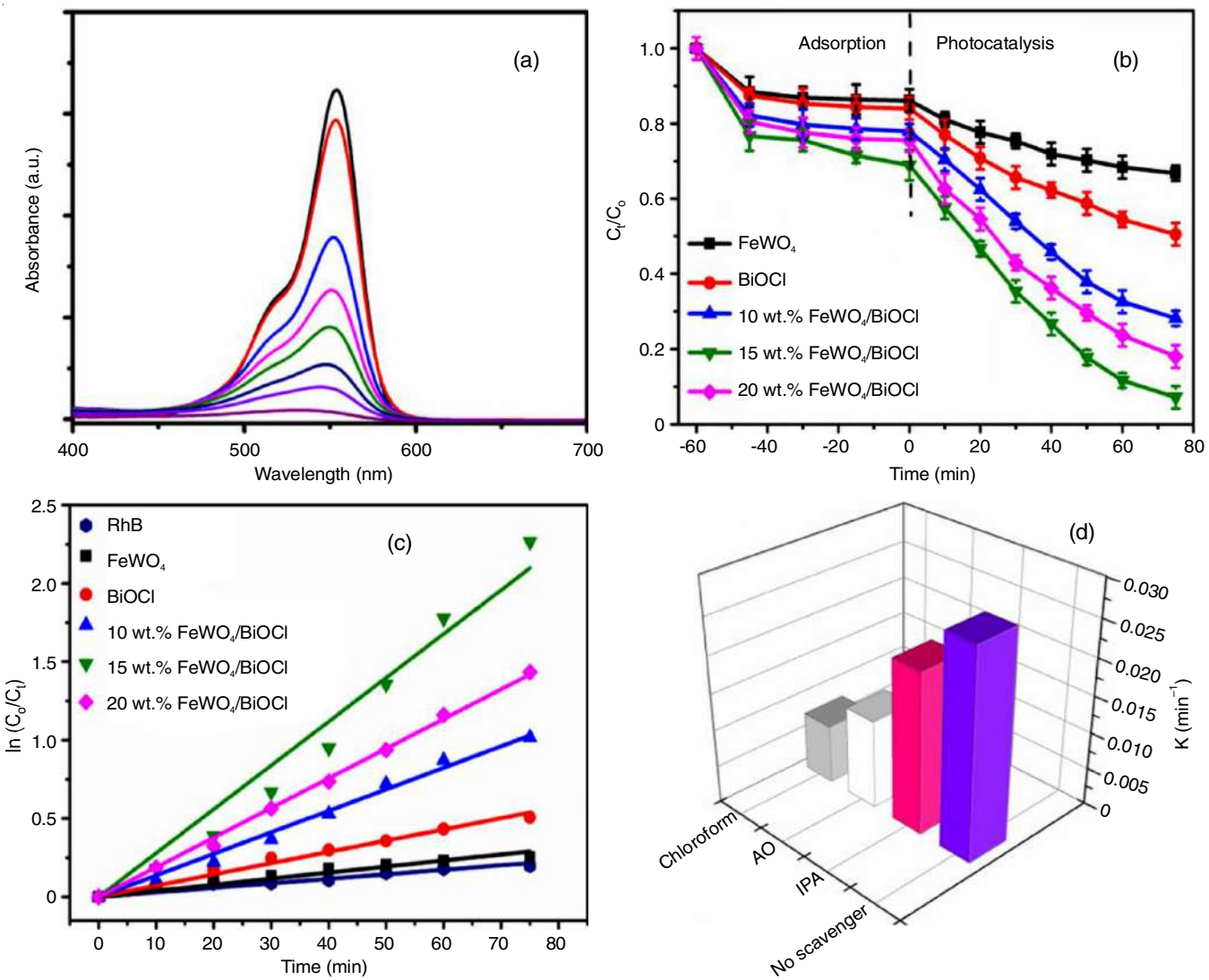

Fig. 4. (a) UV-vis absorption spectrum of RhB solution in the presence of 15 wt.% $FeWO_4$/BiOCl, (b) degradation plot of RhB by $FeWO_4$, BiOCl and $FeWO_4$/BiOCl nanocomposites, (c) corresponding pseudo-first-order kinetic plot and (d) radical trapping experiment for RhB over 15 wt.% $FeWO_4$/BiOCl photocatalyst

results of degradation rate for different batches of $FeWO_4$/BiOCl, $FeWO_4$ and BiOCl are shown in Table-1. The 15 wt.% $FeWO_4$/BiOCl exhibited maximum photocatalytic efficiency, *i.e.* 99% RhB degradation in 75 min of sunlight irradiation, which was six times higher than the pristine BiOCl as photocatalyst. The corresponding rate of degradation by 15 wt.% $FeWO_4$/BiOCl was 0.0279 min^{-1} for RhB. The photocatalytic degradation of pristine $FeWO_4$ and BiOCl were evaluated as 0.0038 and 0.0071 min^{-1}, respectively under same conditions. The improved degradation of RhB by 15 wt.% $FeWO_4$/BiOCl is attributed to the generation of reactive oxygen species (ROS). This has been ascertained from the specific ROS scavenging studies. The RhB solution treated with 15 wt.% $FeWO_4$/BiOCl were treated with ROS scavengers *e.g.* isopropyl alcohol, chloroform and ammonium oxalate [22], as h^+, $O_2^{\bullet-}$ and $^{\bullet}OH$ quenchers, respectively. The photocatalytic degradation kinetics of RhB solutions by 15 wt.% $FeWO_4$/BiOCl photocatalyst in presence of specific ROS scavengers are shown in Fig. 4d. Significantly, the photocatalytic degradation rate of RhB treated with ROS scavengers

TABLE-1
PHOTOCATALYTIC DEGRADATION EXPERIMENTS

Sample name	Adsorption (%)	Degradation (%)	K (min^{-1})
20 wt.% $FeWO_4$/BiOCl	25	82	0.0189
15 wt.% $FeWO_4$/BiOCl	32	98	0.0279
10 wt.% $FeWO_4$/BiOCl	23	72	0.0137
BiOCl	16	50	0.0071
$FeWO_4$	14	34	0.0038
Blank	NA	10	0.0010

decreased than the one without treating with ROS scavengers. Among the ROS scavengers, the batch treated with chloroform exhibited profound decrease in the photocatalytic degradation rate. As chloroform tends to scavenge superoxide radicals, so the negative result in photodegradation of RhB due to addition of chloroform indicates scavenging of *in situ* generated superoxide radicals, which was scavenged by chloroform and resulted in drastic decrease in the photodegradation of RhB dye. This is confirmed by observing decrease in the photodegradation rate

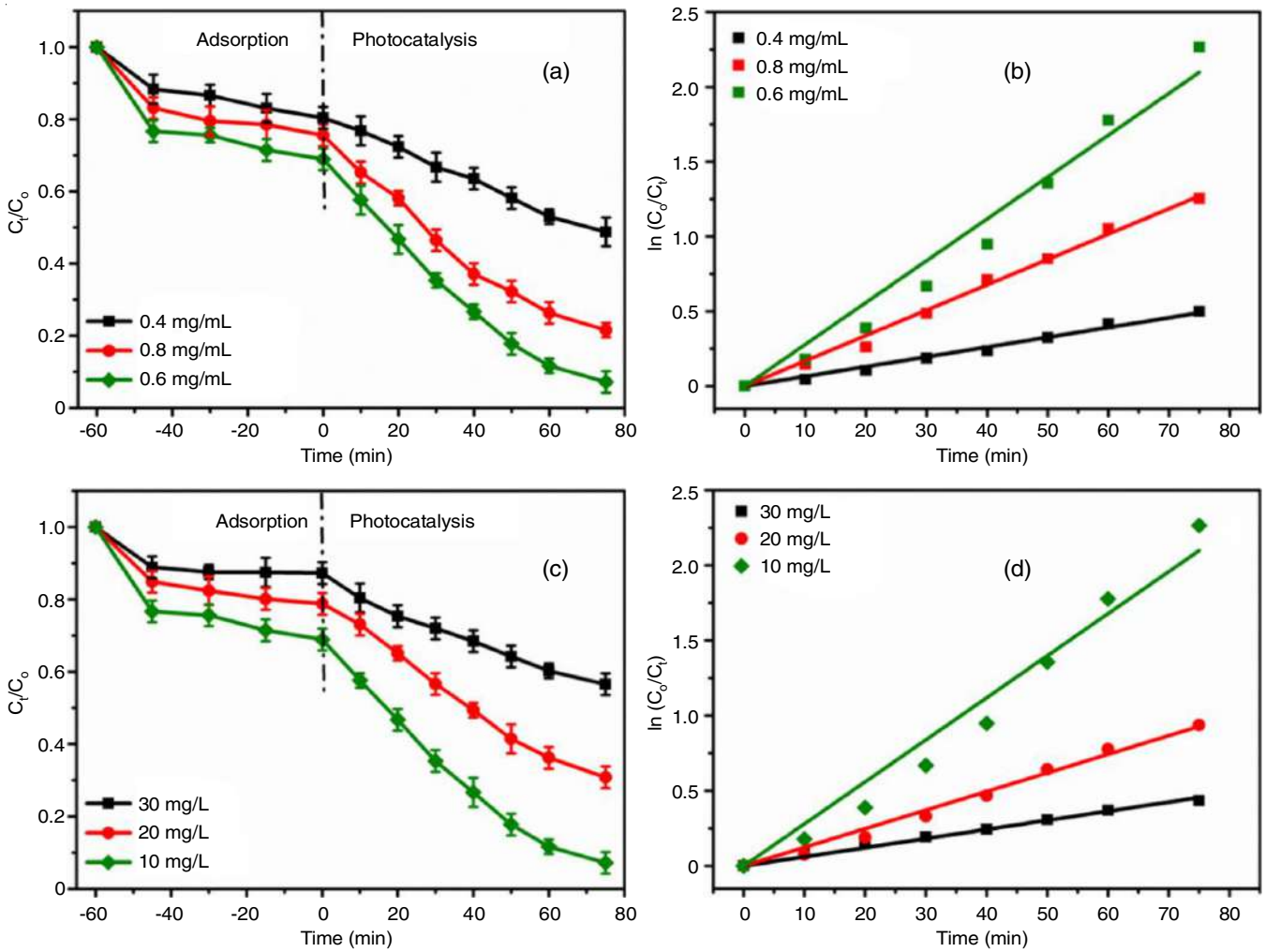

Fig. 5. (a) Effect of photocatalyst dose on the photocatalytic performance on RhB degradation, (b) corresponding first-order kinetics curves, (c) effect of RhB antibiotic concentration on the photocatalytic performance, (d) corresponding first-order kinetic curves

of RhB when holes scavenger, *e.g.* ammonium oxalate was added to the RhB solution (Fig. 4d).

Reusability studies: Reusability of photocatalyst during the photocatalytic degradation plays a significant role in the application. Fig. 6a represents the reusability of 15 wt.% $FeWO_4$/BiOCl photocatalyst for the photodegradation of RhB up to five runs, which reveals an indistinguishable degradation pattern in each run, confirming the higher stability of photocatalyst.

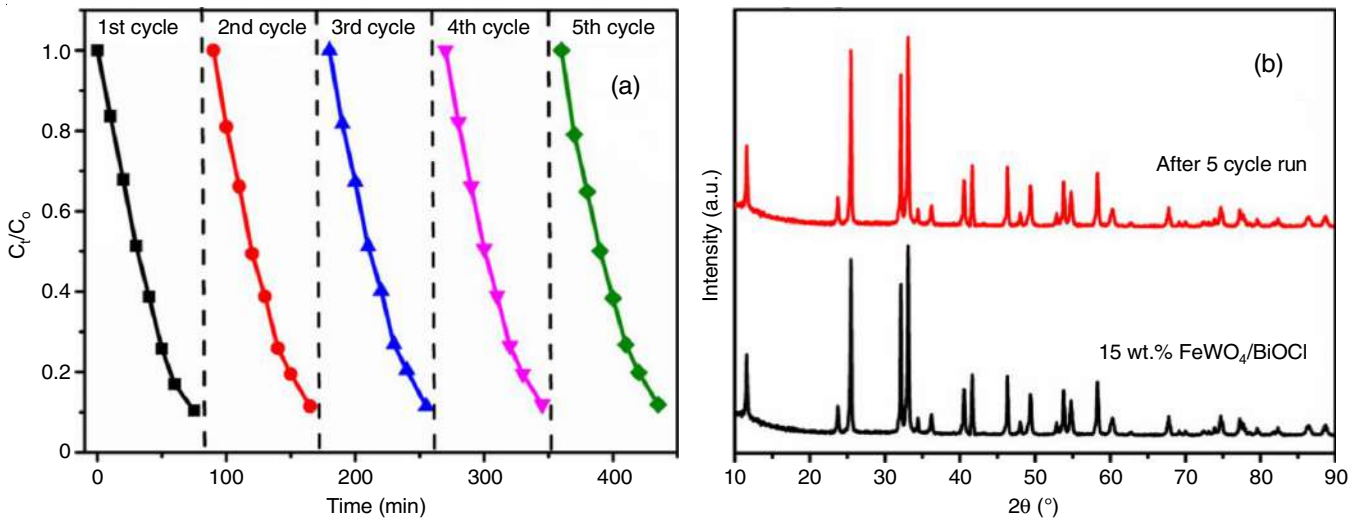

Fig. 6. (a) Recyclability experiment and (b) pXRD pattern of 15 wt.% $FeWO_4$/BiOCl before and after 5 cycle degradation of RhB dye

Unchanged pXRD pattern of the used photocatalyst after 5 cycles further confirm the stability of 15 wt.% $FeWO_4$/BiOCl photocatalyst (Fig. 6b).

Photocatalytic mechanism: The charge carrier route in a heterojunction based photocatalyst is favoured when the band positions of the respective semiconductors are suitably aligned. As the E_{CB} of $FeWO_4$ displays negative (-) potential in comparison to BiOCl, hence, the e^- migrates from the E_{CB} of $FeWO_4$ to the E_{VB} of BiOCl, (type-II heterojunction system). The ECB of BiOCl exhibits a positive potential relative to $O_2^{\bullet-}$ (–0.33 eV), which renders the reduction of O_2 to a superoxide radical anion ($O_2^{\bullet-}$) by electrons in the ECB of BiOCl quite challenging [23]. According to the radical trapping experiment, $O_2^{\bullet-}$ is one of the major active species, which are responsible for degradation of RhB, that cannot be produced according to type-II heterojunction mechanism. The plausible mechanism was proposed for the degradation of RhB using $FeWO_4$/BiOCl heterojunction photocatalyst, as shown in Fig. 7. $FeWO_4$ and BiOCl both generate e^- and h^+ generated by absorption of visible light under exposure of sunlight. In $FeWO_4$/BiOCl heterojunction, the photogenerated e^- in the E_{CB} of BiOCl (e^-_{CB}) would migrate to E_{VB} of $FeWO_4$ to reconnect promptly with the photogenerated holes (h^+_{VB}), while the E_{VB} holes of BiOCl remain on it to oxidize RhB. Furthermore, the electron in the E_{CB} of $FeWO_4$ could effortlessly resettle to the O_2 molecules adsorbed over the surface $FeWO_4$/BiOCl photocatalyst to generate the $O_2^{\bullet-}$ that oxidize RhB. The formation of superoxide radical anion ($O_2^{\bullet-}$) may takes place from the two electron-process from H_2O_2 and by further reaction with holes according to following equation:

$$FeWO_4 + h\nu \longrightarrow e^-_{CB} + h^+_{VB} \quad (3)$$

$$BiOCl + h\nu \longrightarrow e^-_{CB} + h^+_{VB} \quad (4)$$

$$BiOCl\,(e^-_{CB} + h^+_{VB}) + FeWO_4\,(e^-_{CB} + h^+_{VB}) \longrightarrow BiOCl\,(e^-_{CB}) + FeWO_4\,(h^+_{VB}) \quad (5)$$

$$BiOCl\,(e^-_{CB}) + FeWO_4\,(h^+_{VB}) \longrightarrow \text{Recombination} \quad (6)$$

$$BiOCl\,(h^+_{VB}) + RhB_{(aq)} \longrightarrow CO_2 + H_2O \quad (7)$$

$$FeWO_4\,(e^-_{CB}) + O_2 \longrightarrow FeWO_4 + O_2^{\bullet-} \quad (8)$$

$$O_2^{\bullet-} + RhB_{(aq)} \longrightarrow CO_2 + H_2O \quad (9)$$

Cytotoxicity of $FeWO_4$/BiOCl nanocomposites: The cytotoxicity of the $FeWO_4$/BiOCl Nanocomposites was tested using CHO cells at different $FeWO_4$/BiOCl concentrations, *i.e.* 0.1 µg/mL, 0.2 µg/mL, 0.5 µg/mL, 1.0 µg/mL, 5 µg/mL and 10 µg/mL. After 24 h, a cell viability test was conducted by propidium iodide (PI) uptake. In this experiment, the percentage of dead cells has been considered. For $FeWO_4$/BiOCl dose dependent cytotoxicity response has been observed. Although in case of $FeWO_4$/BiOCl the increasing cytotoxicity is observed from concentration 1 µg/mL to 75 µg/mL as shown in Fig. 8. In case of cellular uptake of $FeWO_4$/BiOCl increasing SSC (granularity) was observed in CHO cell line by increasing concentration from 1-100 µg/mL and at higher concentration cell death is observed as shown in Fig. 9.

Conclusion

A novel $FeWO_4$/BiOCl heterogeneous nanocomposites was synthesized by *in situ* hydrothermal method which shows an excellent photocatalytic degradation activity towards RhB under exposure of sunlight. The photocatalytic degradation efficiency of 15 wt.% $FeWO_4$/BiOCl photocatalyst for RhB was much better than BiOCl photocatalyst as rate constant for RhB was about six times better in case of 15 wt.% $FeWO_4$/BiOCl. The structural integrity and photocatalytic efficiency

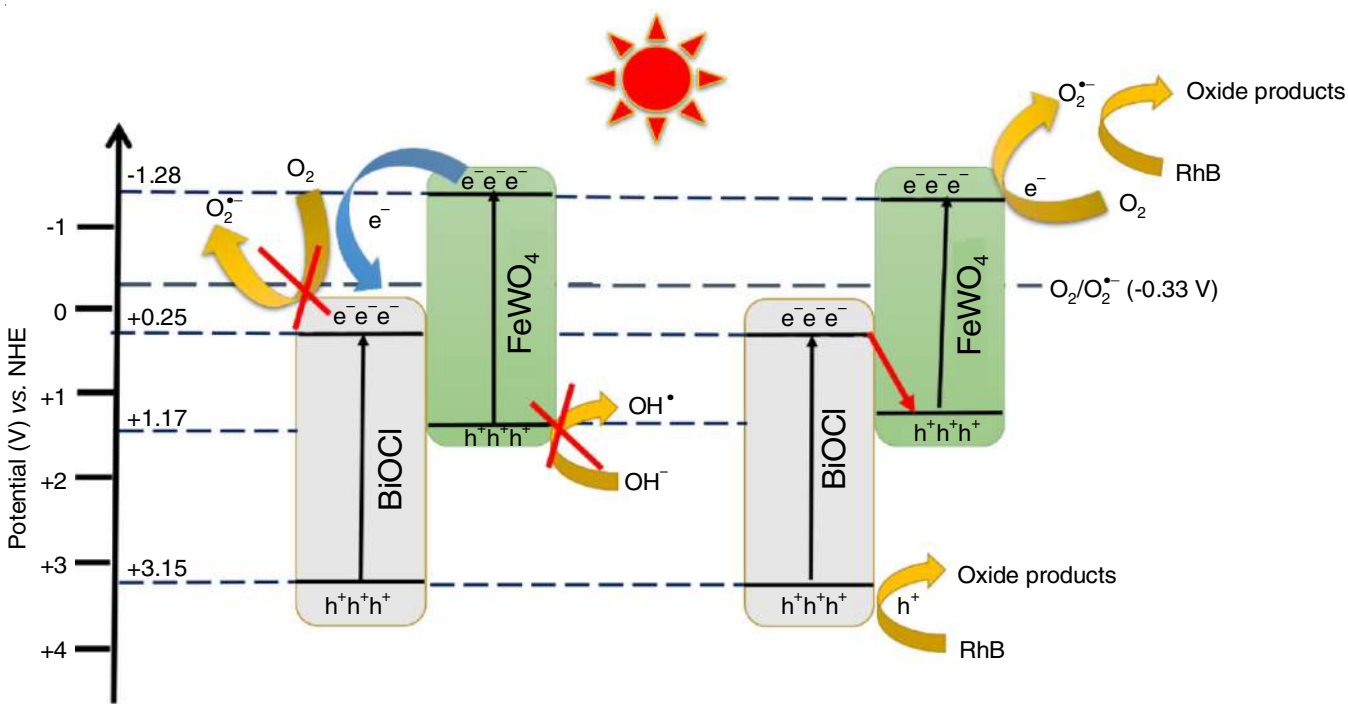

Fig. 7. Possible photocatalytic degradation mechanism of RhB over $FeWO_4$/BiOCl nanocomposite under sunlight irradiation (a) type-II heterojunction, (b) Z-scheme type

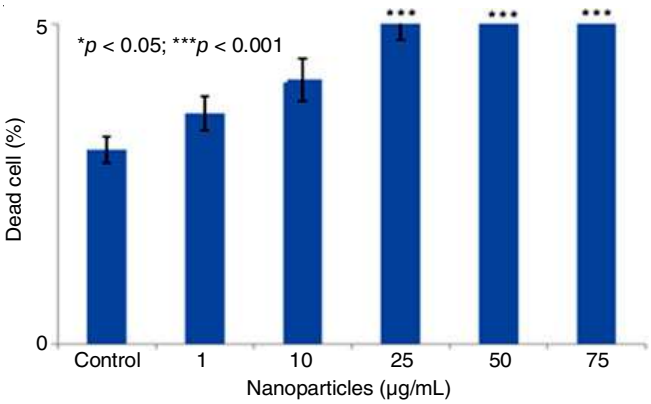

Fig. 8. Percent dead cells as measured by propidium iodide (PI) uptake method using flow cytometry on treatment with nanoparticles

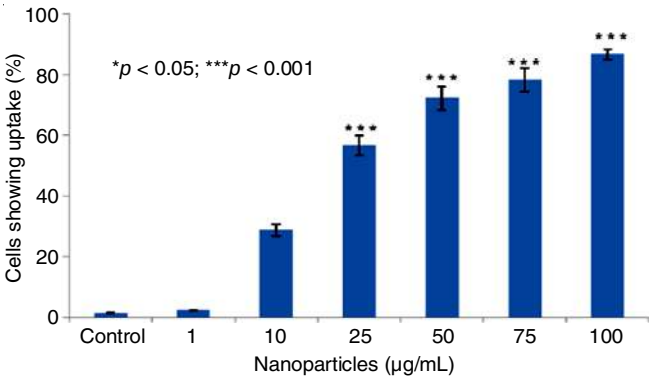

Fig. 9. $FeWO_4$/BiOCl nanoparticles cellular uptake assessed by flow cytometry in CHO cells

of $FeWO_4$/BiOCl nanocomposite remain unaffected after five runs. In addition, cytotoxicity of $FeWO_4$/BiOCl nanocomposite was evaluated by PI and cellular uptake. The cytotoxicity of $FeWO_4$/BiOCl is dose dependent and it increases the % dead cell after 24 h of exposure. In $FeWO_4$/BiOCl, the cytotoxicity increases as the concentration increase from concentration 1 µg/mL to 75 µg/mL. In case of cellular uptake, $FeWO_4$/BiOCl nanocomposites decreases cell viability after 24 h of exposure, as the concentration increase from 1-100 µg/mL.

ACKNOWLEDGEMENTS

The authors are thankful to Prof. R.K. Dwivedi (Dean), Faculty of Engineering, (TMU) Moradabad, India, for his valuable insight and suggestions for this study.

CONFLICT OF INTEREST

The authors declare that there is no conflict of interests regarding the publication of this article.

REFERENCES

1. S. Sharma and A. Bhattacharya, *Appl. Water Sci.*, **7**, 1043 (2017); https://doi.org/10.1007/s13201-016-0455-7
2. F. Saadati, N. Keramati and M.M. Ghazi, *Crit. Rev. Environ. Sci. Technol.*, **46**, 757 (2016); https://doi.org/10.1080/10643389.2016.1159093
3. S. Manzetti and R. Ghisi, *Mar. Pollut. Bull.*, **79**, 7 (2014); https://doi.org/10.1016/j.marpolbul.2014.01.005
4. R. Zhang, J. Tang, J. Li, Z. Cheng, C. Chaemfa, D. Liu, Q. Zheng, M. Song, C. Luo and G. Zhang, *Sci. Total Environ.*, **450-451**, 197 (2013); https://doi.org/10.1016/j.scitotenv.2013.02.024
5. J. Fick, H. Söderström, R.H. Lindberg, C. Phan, M. Tysklind and D.G.J. Larsson, *Environ. Toxicol. Chem.*, **28**, 2522 (2009); https://doi.org/10.1897/09-073.1
6. I. Michael, L. Rizzo, C.S. McArdell, C.M. Manaia, C. Merlin, T. Schwartz, C. Dagot and D. Fatta Kassinos, *Water Res.*, **47**, 957 (2013); https://doi.org/10.1016/j.watres.2012.11.027
7. Q.T. Dinh, E. Moreau-Guigon, P. Labadie, F. Alliot, M.-J. Teil, M. Blanchard and M. Chevreuil, *Chemosphere*, **168**, 483 (2017); https://doi.org/10.1016/j.chemosphere.2016.10.106
8. R. Daghrir and P. Drogui, *Environ. Chem. Lett.*, **11**, 209 (2013); https://doi.org/10.1007/s10311-013-0404-8
9. M.J.F. Calvete, G. Piccirillo, C.S. Vinagreiro and M.M. Pereira, *Coord. Chem. Rev.*, **395**, 63 (2019); https://doi.org/10.1016/j.ccr.2019.05.004
10. K. Qin, Q. Zhao, H. Yu, X. Xia, J. Li, S. He, L. Wei and T. An, *Environ. Res.*, **199**, 111360 (2021); https://doi.org/10.1016/j.envres.2021.111360
11. M. Hojamberdiev, K.I. Katsumata, S.A. Bilmes, N. Matsushita, K. Morita and K. Okada, *Appl. Catal. A Gen.*, **457**, 12 (2013); https://doi.org/10.1016/j.apcata.2013.03.014
12. F. Chen, Q. Yang, J. Sun, F. Yao, S. Wang, Y. Wang, X. Wang, X. Li, C. Niu, D. Wang and G. Zeng, *ACS Appl. Mater. Interfaces*, **8**, 32887 (2016); https://doi.org/10.1021/acsami.6b12278
13. G. Zhang, D. Chen, N. Li, Q. Xu, H. Li, J. He and J. Lu, *Appl. Catal. B*, **250**, 313 (2019); https://doi.org/10.1016/j.apcatb.2019.03.055
14. X. Gao, G. Huang, H. Gao, C. Pan, H. Wang, J. Yan, Y. Liu, H. Qiu, N. Ma and J. Gao, *J. Alloys Compd.*, **674**, 98 (2016); https://doi.org/10.1016/j.jallcom.2016.03.031
15. A.P. Chowdhury and B.H. Shambharkar, *Chem. Eng. J. Adv.*, **4**, 100040 (2020); https://doi.org/10.1016/j.ceja.2020.100040
16. X. Shi, L. Wang, A.A. Zuh, Y. Jia, F. Ding, H. Cheng and Q. Wang, *J. Alloys Compd.*, **903**, 163889 (2022); https://doi.org/10.1016/j.jallcom.2022.163889
17. E. Grilla, M.N. Kagialari, A. Petala, Z. Frontistis and D. Mantzavinos, *Catalysts*, **11**, 650 (2021); https://doi.org/10.3390/catal11060650
18. Z. Zhang, A. Zada, N. Cui,N. Liu, M. Liu, Y. Yang, D. Jiang, J. Jiang, S. Liu, *Crystals*, **11**, 981 (2021); https://doi.org/10.3390/cryst11080981
19. X. Meng, L. Jiang, W. Wang and Z. Zhang, *Int. J. Photoenergy*, **2015**, 747024 (2015); https://doi.org/10.1155/2015/747024
20. F. Qiu, W. Li, F. Wang, H. Li, X. Liu and J. Sun, *J. Colloid Interface Sci.*, **493**, 1 (2017); https://doi.org/10.1016/j.jcis.2016.12.066
21. J. Gao, Y. Gao, Z. Sui, Z. Dong, S. Wang and D. Zou, *J. Alloys Compd.*, **732**, 43 (2018); https://doi.org/10.1016/j.jallcom.2017.10.092
22. G. Kumar, *J. Inorg. Organomet. Polym. Mater.*, **33**, 2710 (2023); https://doi.org/10.1007/s10904-023-02711-y
23. W.H. Koppenol, D.M. Stanbury and P.L. Bounds, *Free Radic. Biol. Med.*, **49**, 317 (2010); https://doi.org/10.1016/j.freeradbiomed.2010.04.011